The effect of enhanced accessibility of acid sites in micro-mesoporous mordenite zeolites on hydroisomerization of *n*-hexane

Jana Pastvova[1, 2], Dalibor Kaucky[1], Jaroslava Moravkova[1], Jiri Rathousky[1], Stepan Sklenak[1]
Maryna Vorokhta[3], Libor Brabec[1], Radim Pilar[1], Ivo Jakubec[4], Edyta Tabor[1], Petr Klein[1], Petr Sazama[1,*]

[1]*J. Heyrovský Institute of Physical Chemistry, Academy of Sciences of the Czech Republic,*
Dolejskova 3, 182 23 Prague, Czech Republic, [*]*E-mail: petr.sazama@jh-inst.cas.cz*
[2]*University of Pardubice, Studentská 95, Pardubice, 532 10, Czech Republic*
[3]*The Institute of Rock Structure and Mechanics, Academy of* Sciences of the Czech Republic,
V Holesovickach 94/41, 182 09 Prague, Czech Republic
[4]*Institute of Inorganic Chemistry, Academy of Sciences of the Czech Republic, Husinec-Rez,*
25068 Rez, Czech Republic

Abstract:

This paper describes a study of the nature and the accessibility of the acid sites in micro-mesoporous mordenite zeolites obtained by desilication and dealumination and analysis of their activity and selectivity in the hydroisomerization of *n*-hexane. The alkaline-acid, acid-alkaline-acid, and fluorination-alkaline-acid postsynthesis treatments were employed for preparation of micro-mesoporous mordenites. The FTIR spectra of adsorbed d_3-acetonitrille, ^{27}Al MAS NMR, HR-TEM, and N_2 adsorption were used for quantitative analysis of the Brønsted and Lewis sites, the coordination of Al atoms and the textural properties. The alkaline treatment causes desilication, preferably occurring along the crystal defects and resulting in the formation of a secondary mesoporous structure characterized by 5-20 nm cavities and the formation of extraframework (Al_{Ex}) species and terminal Si–OH groups. The Al_{Ex} formed by hydrolysis of perturbed or dislodged framework Al easily restrict part of the pseudo-monodimensional channel structure of mordenite. The subsequent removal of Al_{Ex} by mild acid leaching or simultaneous removal of Si and Al atoms by desilication of fluorinated zeolite result in a micro-mesoporous structure with a large number of unrestricted channel openings and lead to a large increase in the accessibility of OH groups for *n*-hexane. Thus, the sequential leaching treatments enable the formation of active acid sites in an environment of non-restricted microporous channels with simultaneous enhancement of accessibility of the active sites and molecular transport. It is shown that the micro-mesoporous structure with high concentration of Brønsted sites of enhanced accessibility directs the hydroisomerization reaction toward high yields of branched isomers and shortening of the main 12-ring channels and that the larger number of channel openings result in an increase in selectivity, limiting nonselective subsequent cracking reactions.

Keywords: Isomerization; n-hexane; micro-mesoporous mordenite (MOR) zeolites; hierarchical structure; desilication

1. Introduction

The isomerization of linear or low-branched alkane hydrocarbons via an intermediate alkene is an important process in oil refining for production of automotive fuels. The hydroisomerization of *n*-hexane transforms the linear isomer with low octane number into branched hexanes with sufficiently high octane numbers, e.g., research octane numbers are 26 and 93 for *n*-hexane and 2,2-dimethylbutane, respectively. The process is typically catalysed by bifunctional Pt/H-mordenite catalysts and its complex mechanism consists dehydrogenation of hexane to a hexene molecule on metallic platinum, skeletal isomerization of the hexene molecule on an acidic Brønsted site and re-hydrogenation of the branched hexene to hexane [1-4]. The acid-catalysed reaction steps determine the overall reaction rate while the dehydrogenation/hydrogenation reactions are usually in thermodynamic equilibrium and practically do not affect the reaction rate of the hydroisomerization [4-5]. Acid sites are located in mordenite zeolites in the small side pockets with eight-membered ring (8-ring) openings and the main large straight channels with 12-ring openings (Figure 1) forming different local reaction environments affecting the confinement of a reactant molecule and corresponding adsorption enthalpy and stabilization of transition states [6-7]. The reaction rate of hydroisomerization of *n*-hexane over mordenites is thus controlled by the concentration of acid sites located in the 8-ring channel-pockets and in the 12-ring main channels with five times higher turnover frequency (TOF) per proton in 8-ring channel-pockets compared with that in 12-ring channels [8].

Nevertheless, the accessibility of 8-ring (2.6 Å × 5.7 Å) compared to 12-ring (6.5 Å × 7.0 Å) channels is diffusion-restricted for *n*-hexane (cf. the size of the channel openings and kinetic diameters of the hexane isomers in Figure 1 [9-12] and the efficiency of the catalytic process is limited by mass transfer effects [5, 13]. Because of their larger kinetic diameter, the branched hexanes diffuse even more slowly than *n*-hexane [14]. The accessibility of acid sites in the current industrial catalysts is enhanced by acid-treated partially dealuminated mordenites with improved textural properties [5]. However, dealumination leads to a decrease in the concentration of Brønsted sites, the formation of Lewis sites and small changes in the micropores [5]. In recent years, considerable efforts have been devoted to improving the pore accessibility and molecular transport of reactants to active sites in micropores, namely in MFI zeolites, to enhance the activity in yielding the desired products in a variety of important acid-catalysed reactions [15-20]. Several approaches have been developed to shorten the length of micropores and thus enhance mass transport by using zeolite nanosheets and nanocrystals [17, 21-22] or zeolites that contain both micro- and mesopores. Micro-mesoporous (hierarchical) zeolites can be prepared by a variety of synthesis or post-synthesis methods, e.g., by confined crystal

growth [15, 23], using polymers as mesoporogens [13], or through post-synthesis desilication or dealumination processes [11, 18, 24-26].

In the present work, we attempted to enhance the accessibility of the active sites by introducing secondary mesoporosity into mordenite zeolites coupled while attempting to preserve a large number of acid sites. The methods for effective formation of secondary mesoporosity through postsynthesis alkaline, alkaline-acid, acid-alkaline-acid and fluorination-alkaline leaching procedures of conventional mordenite zeolites were explored in the preparation of micro-mesoporous zeolites with high concentrations of readily accessible Brønsted acid sites. In contrast to dealumination, controlled alkaline-based treatments of the mordenite framework lead to better preservation of the concentration of Brønsted sites and formation of well-developed secondary mesoporosity. The process was followed in respect to the state of Al, the concentration and accessibility of Brønsted sites and Al-Lewis sites together with changes in the micro-meso texture and how these parameters are reflected in *n*-hexane hydroisomerization over H/Pt-MOR.

2. Experimental

2.1 Preparation of micro-mesoporous H- and Pt/H-mordenite zeolites

Mordenite zeolite (Zeolyst Int., CBV 20A molar Si/Al 12.1), denoted as MOR/12, was used for preparation of micro-mesoporous mordenites using postsynthesis alkaline, alkaline-acid, acid-alkaline-acid, and fluorination-alkaline-acid leaching procedures (Figure 2) and as a standard for comparing catalytic properties. The first series of micro-mesoporous mordenites was prepared using alkaline and alkaline-acid treatments by leaching MOR/12 in an alkaline solution (30 ml 0.2 M NaOH per 1 g mordenite stirred in a beaker at 85 °C for 2 h, sample mm-MOR/8) [27] and subsequent leaching in acid solutions (30 ml 0.1 M oxalic acid per 1 g alkaline treated zeolite stirred in a beaker at 85 °C for 20 h, sample deAl-mm-MOR/9, or 40 ml 0.1 M HNO$_3$ per 1 g alkaline treated zeolite stirred in a beaker at 50 °C for 15 min, sample deAl-mm-MOR/9.5). The second series was prepared using acid-alkaline-acid treatments with dealumination of MOR/12 (30 ml 3 M HNO$_3$ per g mordenite stirred and heated under reflux at 80 °C for 40 min, sample deAl-MOR/16), subsequent desilication (30 ml 0.2 M NaOH per 1 g dealuminated zeolite stirred in a beaker at 85 °C for 2 h, sample mm-deAl-MOR/9.1), and finally mild dealumination (30 ml 0.1 M HNO$_3$ per 1 g zeolite at 50 °C for 15 min, sample deAl-mm-deAl-MOR/13; or 30 ml 0.1 M (COOH)$_2$ per 1 g zeolite at 85 °C for 20 h, sample deAl-mm-deAl-MOR/30). The third series was prepared by fluorination of MOR/12 (5 g

mordenite were impregnated by 15 ml 0.36 M NH_4F at room temperature, stored at RT for 8 h, and subsequently dried at 120 °C for 12 h), subsequent desilication (30 ml 0.2 M NaOH per 1 g fluorinated mordenite stirred in a beaker at 85 °C for 30 min) and calcination at 550 °C for 3 h (sample mm-F-MOR/9.4), with subsequent leaching in acid solutions (30 ml 0.1 M HNO_3 per 1 g zeolite at 50 °C for 15 min, sample deAl-mm-F-MOR-F/13.6).

All the zeolites were ion-exchanged with 0.5 mol.dm^{-3} NH_4NO_3 at RT (1 g of a zeolite per 100 cm^3 of solution, three times over 12 h). Pt was introduced into the zeolites by incipient wetness impregnation with a H_2PtCl_6 solution to yield 1.5 wt.% of Pt. The Pt-impregnated granulated zeolite was activated before the catalytic test in a stream of O_2 at 450 °C for 3 h, then purged by a N_2 stream at 450 °C, followed by cooling down to 250 °C, and finally activated in a mixture of 80 mol% H_2 and 20 mol% N_2 at 250 °C for 1 h.

2.2. Characterization of zeolites

A Bruker AXSD8 Advance diffractometer with CuKα radiation in Bragg–Brentano geometry with a graphite monochromator and a position sensitive detector (Våntec-1) was used to record the X-ray powder diffraction (XRD) patterns. The porosity of the modified mordenites was determined by analysis of the adsorption isotherms of nitrogen at the boiling point of liquid nitrogen at 77 K. Before the adsorption experiment, the samples were outgassed at 240 °C for at least 24 hours to ensure complete cleaning of the surface. The experiments were carried out using an ASAP 2010 apparatus (Micromeritics). The volume of micropores and the external surface area were determined by the Broekhoff-de Boer t-plot. The total pore volume was determined by converting the adsorption at the relative pressure of 0.8 to the volume of liquid nitrogen. The relative pressure around 0.8 for practically all the investigated samples is high enough for complete filling of the pores and low enough to have substantial proportion in the interstitial space. The volume of mesopores was finally calculated by subtracting the volume of micropores from the total pore volume (at the relative pressure of 0.8). The crystal morphology was analysed using a JEOL JSM-5500LV scanning electron microscope (SEM), (Figure S1). High-resolution transmission electron microscopy (HR-TEM) was carried out on a JEOL JEM 3010 microscope operated at 300 kV (LaB_6 cathode, point resolution 1.7 Å). The length of the diffusion path in the mordenite channel in the crystal with the mesopores was estimated using a model approach as follows: The crystal size is 80 x 80 x 80 nm and the volume corresponding to the mesopores is 0.09 cm^3 g^{-1}. Two cases were modeled: either 18 mesopores of a 8 nm diameter or 72 mesopores of a 4 nm diameter. The mesopores of 80 nm in the length were randomly positioned and oriented along one of the crystal axes. Three cases of the diffusion

paths were considered: the mordenite channel connects (i) one mesopore with the external surface of the crystal, (ii) two mesopores and (iii) two external surfaces. One million simulations was used employing a pseudo-random number generator. The chemical compositions of the parent and prepared Pt-zeolites were determined by X-ray fluorescence spectroscopy using a PW 1404 instrument (Philips). The FTIR spectra of the zeolites evacuated at 450 °C for 3 h were recorded at RT on a Nicolet Nexus 670 FTIR spectrometer operating at 2 cm^{-1} resolution by collecting 256 scans for a single spectrum. The adsorption of d_3-acetonitrile (13 mbar CD_3CN at RT for 20 min with subsequent evacuation for 15 min at RT) was used for analysis of the H-mordenites. The characteristic IR bands of the C≡N vibrations and the extinction coefficients ε_B = 2.05 cm.μmol^{-1} and ε_L = 3.60 cm.μmol^{-1} [28] were used for determination of the concentrations of acidic Brønsted and Lewis sites. The adsorption of n-hexane (1.4 Torr n-hexane at RT for 20 min with gradual desorption to 0.005 Torr at RT) was used to estimate the accessibility of the OH groups of the mordenites for n-hexane. The difference between the intensity of the absorption bands of the OH groups in the spectra of the dehydrated mordenites and the spectra after adsorption of n-hexane provided information on the accessibility of the OH groups in mordenite. The desorption of n-hexane from the samples of microporous (MOR/12) and micro-mesoporous (deAl-mm-MOR/9.5) mordenites was followed by using a Nicolet 6700 FTIR spectrometer and an IR cell equipped with NaCl windows and connected to a vacuum line and n-hexane-dosing set up. The self-supported wafers with thickness < 10 mg.cm^{-2} were evacuated prior the measurement at 450 °C for 3 h. The time-resolved in situ FTIR spectra were recorded at a resolution of 1 cm^{-1} collected at a 0.2 s interval. The desorption of n-hexane was monitored after equilibration with n-hexane at a partial pressure 2.5 Torr at RT for 20 min and very fast decrease in the partial pressure from 2.5 to 1.5 Torr. Solid state ^{27}Al and ^{29}Si MAS NMR experiments were carried out on a Bruker Avance 500 MHz Wide-Bore spectrometer (11.7 T) equipped with 4 mm double-resonance MAS NMR probe-head. High-power decoupling pulse sequence with a p/12 (0.7 μs) excitation pulse, 1 s relaxation delay and rotation speed of 12 kHz were employed for measurement of the ^{27}Al MAS NMR spectra of fully hydrated samples. The chemical shifts were referred to an aqueous solution of $Al(NO_3)_3$. ^{29}Si MAS NMR single pulse spectra of hydrated zeolites were measured at a rotation speed of 7 kHz, with a $\pi/6$ (1.7 μs) excitation pulse and relaxation delay of 30 s for single pulse spectra. The framework aluminum content (Si/Al$_{FR}$) was estimated from the intensity of the ^{29}Si NMR resonances according the equation Si/Al$_{FR}$ = I/(0.25 I$_1$ + 0.5 I$_2$), where I, I$_1$, and I$_2$ correspond to the total, Si(3Si,1Al), and Si(2Si,2Al) intensities, respectively [29-30].

2.3. Catalytic experiments

The isomerization of *n*-hexane to the corresponding *iso*-hexanes was performed in a glass flow-through U-shaped reactor with spiral on the inlet part to enable pre-heating of the reactants, where the catalyst was supported inside reactor on a porous-glass solid bed. Typically the reactor was filled with 0.5 g of the catalyst in the form of a grained solid, 0.25-0.5 mm particle size fraction. The activation was performed before each catalytic test; it consisted of two steps: first, i) the Pt-impregnated zeolite was activated by a stream of O_2 at 450 °C/3h and then briefly (0.25h) purged by N_2 at 450 °C; then temperature was decreased to 250°C and secondly ii) reduced under 250 °C by a mixture of 80% H_2 + 20% N_2 for 1 h. Then the *n*-hexane was co-fed into the same feed of 79% H_2 + 20% N_2 by using a conventional saturator kept at the appropriate temperature. The total gas flow was thus adjusted to 66 $cm^3.min^{-1}$, which corresponded to GHSV 5 000 and WSHV 0.25 h^{-1}. The temperature in the reactor was measured with an immersed thermocouple and set-up at the studied temperature in the 125 – 325 °C range. The composition of the outlet products, consisting of *n*-hexane, branched hexanes and low molecular-weight products (i.e.: C_1, C_2, C_3, C_4 and iso-C_4, C_5 and iso-C_5) was analysed by an on-line sampling GC (Finnigan 9001), equipped with a 50 m × 0.32 mm × 5 μm Al_2O_3/KCl column and detection enabled with a conventional FID detector. Steady-state conditions were usually achieved within 0.5 - 1 h of time-on-stream. The conversion and yield were expressed as:

conversion $=$ $C_{0,n\text{-}C6} - C_{n\text{-}C6}$ / $C_{0,n\text{-}C6}$ × 10^2 (%)

yield $=$ $C_{iso\text{-}C6}$ / $C_{0,n\text{-}C6}$ × 10^2 (%)

where: The $C_{0,n\text{-}C6}$ was the concentration of *n*-hexane at the reactor inlet, while the $C_{n\text{-}C6}$ and $C_{iso\text{-}C6}$ were the concentrations of *n*-hexane and of branched hexanes at the reactor outlet.

3. Results

3.1 Structural analysis

3.1.1 Effect of dealumination of microporous mordenite on the concentration, nature and accessibility of acid sites

The microporous MOR/12 parent zeolite is characterised by well-developed crystalline structure (Figures 3, S1 and S2) with the microporous volume 0.19 $cm^3.g^{-1}$ (Table 1 and Figures 4 and S3) and the presence of the majority of the Al in the framework in tetrahedral coordination (Figure S4), (for details see the Supporting Information). The FTIR spectra of the OH groups and adsorbed d_3-acetonitrile together indicate a slightly predominant concentration of Brønsted

sites in the 12-ring compared to 8-ring channels, compensating the negative charge of regularly tetrahedrally coordinated Al in the framework, and a low concentration of Lewis acid sites (Table 2 and Figures 5 and S5). Observation of the intensity of the infrared bands corresponding to OH groups in 8-ring and 12-ring channels upon introduction of *n*-hexane (Table 2 and Figure S6) was used for estimation of the accessibility of OH groups located in the distinct channels. The band attributed to OH groups in the 8-ring channels of MOR was almost unperturbed after adsorption of *n*-hexane, indicating low accessibility of these OH groups for the probe molecule at RT. This is in accordance with the observation of very low accessibility of the acid sites located in 8-ring channels reported by Eder et al. [31]. Both the experimental [32-34] and theoretical studies [35] of mordenite zeolites showed approximately 1/3 of the Brønsted hydroxyl groups heading toward the centre of 8-ring and centre of the side pocket, which is non-accessible for larger molecules. This number seems to be independent of the Si/Al ratio [36] and is a result of the distribution of Al atoms in the four tetrahedral sites of mordenite [32]; this corresponds well to 64.1% the accessible OH groups for *n*-hexane in H-MOR/12 (Table 2).

After partial dealumination of the framework of the parent mordenite zeolite by 3 M HNO_3, the Si/Al ratio was increased from 12 to 16 with a corresponding decrease in the concentration of the Brønsted sites, accompanied by an increase in the ratio of Lewis/Brønsted sites (Table 2) and a significant increase in the absorption bands at 3 727 cm^{-1}, corresponding to internal silanol groups (Figure 5). The decrease in the concentration of the Brønsted sites and the increase in the band of internal silanol groups are consistent with the removal of the tetrahedrally coordinated framework Al atoms and the formation of four internal SiOH groups terminating the framework oxygen atoms. The structural changes induced by dealumination of mordenite zeolites have been described well in the scientific literature [5, 9, 37]. Removal of the framework Al atoms by acid leaching with nitric acid has been reported to result in secondary micropores that are larger than the main channels [5, 37] or the formation of small mesopores [5], improving the accessibility of the Brønsted OH groups remaining after dealumination in the side pockets. The similar adsorption/desorption branches of N_2 sorption without a hysteresis loop for both MOR/12 and deAl-MOR/16 indicate the absence of a significant volume in intra-crystalline mesopores. The adsorption of *n*-hexane on deAl-MOR/16 caused a dramatic decrease in the intensity of the absorption bands of OH groups that clearly show that the Brønsted acid sites remaining in the deAl-MOR/16 sample zeolite after dealumination are readily accessible for the *n*-hexane molecule (>90%), (Table 2). The absence of mesopores, the increased accessibility of the OH groups and the presence of internal silanol groups indicates that extraction of the framework Al atoms primarily induced changes in the distribution of the

sizes and/or the connectivity of the microporous channels. However, in addition to appreciable textural changes, these structural changes caused a significant decrease in the concentration of the Brønsted acid sites to about half and an increase in the ratio of Lewis/Brønsted sites.

3.1.2 Effect of desilication on structure of mordenite

TEM images of the alkaline-leached zeolite mm-MOR/8 (Figure 3) clearly show that the treatment resulted in extensive formation of a secondary mesoporous structure characterized by numerous cavities about 5-20 nm in size in the microporous crystals. The adsorption isotherms of desilicated mm-MOR/8 zeolite (Figure 4) exhibit a hysteresis loop typical for mesopores and adsorption in the zeolite micropores with a significant decrease in the volume of the micropores from 0.19 to 0.06 $cm^3.g^{-1}$ (Table 1). The preservation of the crystalline structure of mm-MOR/8, which is obvious from the X-ray diffraction patterns (Figure S2) and indirectly from the ^{29}Si MAS NMR spectrum (Table 1), and the lattice fringes in the HR-TEM images (Figure 3) indicate that the decrease in the microporous volume is not associated with collapse of the zeolitic structure but with blocking of the channel openings by AlO_x extraframework plugs formed in the mesopores after desilication [19]. The extraframework Al species (Al_{Ex}) formed in the mesopores during desilication by hydrolysis of perturbed or dislodged framework Al enrich the surface [38] and can easily block a significant part of the pseudo-monodimensional channel structure of mordenite [19]. The presence of Al_{Ex} in mm-MOR/8 is obvious from i) the broadening and decreasing of the symmetry of the signal at 55 ppm in the ^{27}Al MAS NMR spectra (Figure S4) characteristic of variously perturbed Al species in the less-ordered environment compared to ideal tetrahedral coordination of Al atoms in the zeolite framework [39-45], ii) the additional spectral component around 3650 – 3670 cm^{-1} (Figure 5) due to OH groups bound to extra-framework and/or perturbed framework Al atoms [46-48], iii) a higher framework Si/Al ratio estimated from the ^{29}Si MAS NMR spectra compared to the value obtained from chemical analysis (Table 1) and iv) a significant decrease in the concentration of Brønsted OH groups from 1.06 to 0.44 $mmol.g^{-1}$ determined from the FTIR spectra of adsorbed d_3-acetonitrile.

Desilication of the partially dealuminated mordenite (deAl-MOR/16) resulted in better developed secondary mesoporous structure compared to desilication of the parent mordenite, as indicated by higher and continuously increasing adsorption of N_2 at the relative pressures 0.1 – 0.8 and a hysteresis loop in the adsorption/desorption branches of the isotherm (Figure 4). After the alkaline treatments, the mesoporous volume increased to 0.08 and 0.11 $cm^3.g^{-1}$ for mm-MOR/9 and mm-deAl-MOR/9.1, respectively (Table 1). It is well established that the presence of framework Al atoms stabilizes a neighbouring siliceous part of the crystal and the

extraction of Si is hindered for low Si/Al ratios [25, 49]. Consequently, the lower content of Al in the framework of deAl-MOR/16 increased the susceptibility towards leaching of the framework Si atoms. Desilication is also preferred more along crystal defects [50], which were densely created during the partial dealumination of the parent zeolite, and which are reflected in the FTIR spectrum of deAl-MOR/16 in the absorption bands at 3727 cm^{-1} of the internal silanol groups. The preferred desilication in the internal Si-related defects is manifested in a decrease in the intensity of the absorption at 3727 cm^{-1} in the spectra of mm-deAl-MOR/9.1 compared to deAl-MOR/16. Thus, desilication is clearly enhanced upon prior partial dealumination of the microporous zeolite as a result of the higher susceptibility of the zeolite towards leaching at lower concentrations of framework Al atoms as well in the presence of the framework defect sites. The analysis of N_2-sorption isotherms by the Broekhoff-de Boer t-plot shows a decrease in the micropore volume after desilication from 0.19 cm^3.g^{-1} in the parent zeolite to 0.06 and 0.15 cm^3.g^{-1} for mm-MOR/9 and mm-deAl-MOR/9.1, respectively (Table 1). It is probable that a lower concentration of Al in the parent zeolite and/or more developed mesoporosity providing a larger number of openings of the pseudo-monodimensional channels lead to lesser blocking of the micropores in the mm-deAl-MOR/9.1 sample.

3.1.3 Effect of mild acid treatment on the porous structure and accessibility of acid sites in desilicated mordenite

Our recent study [19] on the formation of secondary mesoporosity through postsynthesis sequential leaching procedures demonstrated that the Brønsted active sites located in the environment of non-restricted micropores and accessible through mesopores can be obtained by alkaline and subsequent mild-acid leaching. Treatment of mm-MOR/8 using 0.1 M oxalic acid under mild conditions (deAl-mm MOR/9) resulted a very slight increase in the molar Si/Al ratio, a significant increase in the micropore volume from 0.06 to 0.13 cm^3.g^{-1} and further extended the volume of mesopores (Table 1), a significant increase in the concentration of Brønsted sites from 0.44 to 0.81 mmol.g^{-1} and Levis sites from 0.14 to 0.35 mmol.g^{-1} (Table 2), disappearance of the lowering symmetry of the signal at 55 ppm in the ^{27}Al MAS NMR spectra (Figure S4), and elimination of the absorption band at 3650 – 3670 cm^{-1} due to Al-OH groups (Figure 5). These findings clearly indicate that the extra-framework and/or perturbed framework Al species formed in mesopores after desilication and blocking part of the micropores were removed by acid leaching. The increase in the concentrations of the acid sites indicates that the leaching selectively removed the extraframework tetrahedrally coordinated

$AlO_x/(OH)_y$ species blocking the micropores, whereas the framework Al atoms associated with bridging OH groups were barely affected.

Acid leaching of mm-MOR/8 using 0.1 M nitric acid resulted in slightly more pronounced structural changes compared to the treatment using oxalic acid. Nitric acid, as a stronger dealumination agent [51], caused a moderately greater increase in the molar Si/Al ratio, the same increase in the micropore volume from 0.06 to 0.13 $cm^3.g^{-1}$ and further extension of the mesoporous volume to 0.12 $cm^3.g^{-1}$ (Table 1). A lower concentration of Brønsted sites 0.55 $mmol.g^{-1}$ indicates that part of the framework Al atoms was extracted from the framework and/or perturbed by the treatment in nitric acid. The removal of extraframework Al in the deAl-mm-MOR/9 sample by oxalic acid caused only minor changes in the availability of OH groups compared to the parent zeolite (Table 2). A significant increase in the accessibility of the OH groups (~80%) occurred after slight dealumination of the zeolite framework in the deAl-mm-MOR/9.5 sample by nitric acid. It seems that desilication with subsequent removal of extraframework Al can lead to shortening of the main 12-ring channels, but the number of new channel openings created in mesopores is not large enough for significant enhancement of the accessibility of the OH groups in 8-ring side pockets.

Partial dealumination of mm-deAl-MOR/9.1 using 0.1 M nitric acid caused similar changes to the dealumination of mm-MOR/8; however, they are less pronounced, i.e. opening of restricted micropores with an increase in the volume of micropores from 0.15 to 0.19 $cm^3.g^1$ and increase in the concentration of Lewis sites from 0.22 to 0.45 $mmol.g^{-1}$. The concentration (0.43 $mmol.g^{-1}$) and accessibility of Brønsted acid sites (~ 92%) are very comparable with deAl-MOR/16. Thus the desilication of deAl-MOR/16 with subsequent removal of Al_{Ex} by mild acid leaching resulted in deAl-mm-deAl-MOR/13 with well-developed mesoporous structure and with similar concentration and accessibility of OH groups for *n*-hexane as the starting deAl-MOR/16 before the subsequent alkaline-acid treatments.

The hydrolysis of Al-O and Si-O bonds in the 8-ring (formed by T2 and T4 atoms) during acid and alkaline treatments results in dislodgement of the T atom from the framework position and dramatic changes in the local arrangement. Figure 6 illustrates how the openings of two neighbouring side-pockets in MOR zeolite can be altered by the removal of one T atom in the T2 or T4 sites. The extraction of the T4 atom leads to a merging of the two 8-ring providing a large void space enabling a diffusion of large molecules, e.g. benzene [52]. The extraction of the T2 atom could possibly provide a large deformed elongated ring, however, previous reports indicate that the extraction is site specific and the dealumination of T4 is strongly favoured [52-54]. The creation of these open connections by the preferable extraction of

Al atoms from the T4 sites explains the dramatic increase in the accessibility of the bridging of OH for hexane even after very mild dealumination of the mordenite framework.

3.1.4 Effect of fluorination-alkaline treatment on the porous structure and accessibility of acid sites in mordenite

Recently, Yu et al. [55] showed that impregnation of microporous ZSM-5 zeolite with an aqueous solution of NH_4F prior leaching by a solution of NaOH increases the susceptibility of the zeolite towards leaching of framework Al atoms and provides controlled extraction of both Al and Si atoms. We modified the procedure for alkaline treatment of fluorinated mordenites and obtained the mordenite zeolite mm-F-MOR/9.4 with the mesopore volume increased to 0.09 $cm^3.g^{-1}$ and the volume of the micropores concurrently slightly decreased to 0.14 $cm^3.g^{-1}$ indicating the formation of secondary mesoporosity and opening of non-restricted channel openings of the preserved microporous structure. In addition to the small near circular bright areas reflecting formation of intracrystalline mesoporosity, HR-TEM images (Figure 3) also show mesopores formed along boundaries and intergrowths. The dissolution or etching along boundaries and intergrowths and the indiscriminate dissolution of Al and Si are characteristic of chemical etching with fluoride ions in NH_4F-HF [56] and Al-directed dissolution of siliceous areas is typical for alkaline treatment [57]. Two modes of the formation of the mesoporous structure were also reported by Svelle et al. [50] for standard desilication. They demonstrated the creation of mesopores both as a consequence of Al-directed dissolution of siliceous areas and selective dissolution or etching along boundaries, intergrowths, and defects within each particle. HR-TEM images of mm-F-MOR/9.4 show concomitant contribution of both modes of mesopores formation. The slight shift of the maximum of peak at about 55 ppm in the ^{27}Al MAS NMR spectra (Figure S4) reflects changes in the coordination and local surroundings of the Al sites and/or a site specific dealumination of the individual T sites [52-54]. The concentration of Brønsted and Lewis sites, 0.6 and 0.24 $mmol.g^{-1}$, respectively, determined by adsorption of d_3-acetonitrile, and high accessibility (>90%) of bridging OH groups for n-hexane molecule (Table 2) for the mm-F-MOR/9.4 sample show that the desilication of fluorinated mordenite zeolite yields a micro-mesoporous structure with high concentration of readily accessible acid sites. The development of secondary mesoporosity and preservation of microporosity via concurrent extraction of SiO_2 and smaller amount of Al is enabled by transformation of a fraction of Si-O-Al into the framework as F-bearing tetrahedral Al entities after fluorination [55]. The presence of F-bearing tetrahedral Al species which are readily dislodged in alkaline medium [55] and Al sites in Si-O-Al entities with persistent resistance to alkaline treatment

enabled controlled Al and Si extraction during the alkaline treatment. The finding that this treatment significantly improved the accessibility of OH groups for *n*-hexane is of great importance. The simultaneous removal of Si and Al atoms and smaller size of part of the formed mesopores with possibly a larger number of new channel openings results in a large increase in the accessibility of the OH groups for *n*-hexane.

3.1.5 Effect of mesoporosity on the pore length

In order to illustrate the effect of mesoporosity on the reactant transport a model showing the shortening of the main 12-ring channels was made and the desorption of *n*-hexane was analysed for the microporous and a representative micro-mesoporous mordenite (Figure 7). The model is based on the obtained SEM, HR-TEM and N_2 adsorption data considering the mesoporous volume 0.09 cm^3 g^{-1}, which is approximately 15% of the total volume of the crystal, and the crystal size 80 nm. Two cases were modeled with randomly positioned mesopores of diameter 4 or 8 nm oriented along one of the crystal axes and connected to the external surface of the crystal. The mesopores that communicate with the external surface of the mordenite crystal are observed in the high resolution TEM images and the spatial arrangement of the mesopores in the entire void volume of the crystal was demonstrated by Milina et al. [58] using the positron annihilation lifetime spectroscopy for micro-mesoporous zeolites prepared by desilication using the same amount and the concentration of NaOH solution. Three cases of the diffusion paths were considered: the mordenite channel connects (i) one mesopore with the external surface of the crystal, (ii) two mesopores, (iii) two external surfaces (i.e., the diffusion path 80 nm) if there is no mesopore present. One million simulations using a pseudo-random number generator yielded the diffusion paths of 42 and 39 nm for the mesopores of the 8 and 4 nm diameters, respectively. The diffusion path depends only slightly on the diameter of the mesopores since only approximately 15% of the crystal are removed and a majority of the crystal is not influenced by the mesopores.

The series of FTIR spectra recorded during transient desorption of *n*-hexane induced by a very fast decrease in the partial pressure of *n*-hexane from 2.5 to 1.5 Torr are shown for MOR/12 and deAl-mm-MOR/9.5 in Figure S6. The partial pressure 1.5 Torr provides the loading of one *n*-hexane molecule per acid site while *n*-hexane molecules weakly interacting with the inert channel walls are also present at the partial pressure 2.5 Torr. Under such decrease in the partial pressure, the changes in transport can be associated with the alterations of the pore structure rather than with desorption of *n*-hexane from the acid sites. The higher desorption rate observed for the micro-mesoporous deAl-mm-MOR/9.5 compared to microporous MOR/12 is

thus consistent with the effective reduction of the crystal domain by the introduction of the mesopores communicating with both the micropores and connected with the external surface. The enhanced transport in the micro-mesoporous zeolite can be, however, also affected by a contribution from a complex interplay of changes in the local structure of microporous channels and the channel openings [59].

3.1.6 Structure of Pt species

Ribeiro et al. [60] showed that the reaction rate in the hydroisomerization reaction is practically independent of the surface of the metallic platinum clusters for platinum loadings from 0.5 to 6 wt. % in Pt-faujasite zeolites. Consistently, Van de Runstraat et al. [61] showed that the hydrogenation/dehydrogenation functions of platinum was not rate-determining for Pt/H-*BEA with platinum loading of ~ 1.5 wt. %. Accordingly, to ensure that the dehydrogenation/hydrogenation reactions do not limit the overall alkane hydroisomerization, all the Pt/H-MOR catalysts were prepared with a concentration of 1.5 wt. % Pt and the dispersity of the platinum clusters was checked using HR-TEM and FTIR spectra of adsorbed CO. Well-dispersed platinum clusters with particle sizes ~1 - 20 nm located on the external surface of the zeolite crystals were observed in the HR-TEM images of all the microporous and micro-mesoporous Pt-MOR zeolites (Figure S7). The broad distribution of the Pt cluster sizes is typical for Pt-zeolites prepared by conventional incipient wetness impregnation. Similar intensities of the absorption bands of the hydroxyl group in the FTIR spectra before and after impregnation of the mordenites with platinum indicate that the Pt reduced in a hydrogen atmosphere is not coordinated in cationic sites to a significant extent (not shown). The FTIR spectra of CO adsorbed on microporous and micro-mesoporous Pt/H-MOR zeolites (Figure S8) exhibit the presence of a broad absorption band at 2078 cm^{-1} characteristic for reduced Pt metallic clusters 1-20 nm in size [62-63] located on the external surface of the zeolite crystal. The reduction of Pt into the zero-valent oxidation state of metallic Pt is also indicated by the absence of the absorption bands at 2170 - 2150 cm^{-1} and at 2130 - 2140 cm^{-1} characteristic of CO interacting with Pt^{2+} counterions and $Pt_n^{\delta+}$ clusters, respectively [62-63]. Thus all the Pt/H-MOR contains well-dispersed platinum in the form of metallic clusters that can provide sufficient hydrogenation/dehydrogenation reactions occurring for the employed Pt loadings much more rapidly than isomerization reaction on acid sites regardless of the specifics of their structure for all the Pt/H-zeolite catalysts [60, 64].

The presence of the secondary mesoporous structure can possibly increase the proximity between the metallic platinum and the Brønsted sites. The effect of nanoscale proximity of

metallic sites and acid sites on the hydroconversion of hydrocarbons was recently assessed by Zecevic et al. [65]. They showed that the closest proximity between the metal and the Brønsted acid sites in zeolites does not provide improved catalytic properties in hydrocracking reactions. It is in line with the results of our study on hydroisomerization [66], where we analysed whether the activity of Pt/H-MOR zeolite is affected by the proximity of Pt species and acid sites using the samples of H-MOR/12-Pt/Al_2O_3 prepared as mechanical mixtures of the protonic form of the zeolite and Pt/Al_2O_3. The yields were practically identical for both the Pt/H-MOR and H-MOR/12-Pt/Al_2O_3 with platinum metal deposited on either the zeolite or alumina [66].

3.2 Hydroisomerization of n-hexane

3.2.1 Hydroisomerization over microporous, desilicated and partially dealuminated-desilicated mordenites

Figure 8 depicts the yields of branched hexane isomers (2-methylpentane, 3-methylpentane, 2,2-dimethylbutane and 2,3-dimethylbutane) and C_1-C_5 by-products (methane, ethane, propane, butanes and pentanes) as a function of the reaction temperature in the hydroisomerization of *n*-hexane over the microporous and micro-mesoporous Pt/H-MOR zeolites. The yields of the individual products at 225 and 250 °C are listed in Table 3. With microporous MOR/12, the conversion first started to increase at a temperature of approximately 150 °C and reached a maximum of 58% at approximately 275 °C before declining again due to non-selective cracking reactions, as is indicated by the steadily increasing conversion of *n*-hexane and yield of C_1-C_5 by-products. The desilication of the parent sample resulted in little improvement in conversions over the entire temperature range, passing through a maximum at 250 °C with the yields increasing from 53.0 to 59.2% and from 9.6 to 11.5% for all the branched and di-branched hexanes, respectively, then declining due to non-selective cracking at higher temperatures. The catalytic behaviour of the mm-MOR/8 sample is in accordance with the findings of Monteiro et al. [67], showing that the desilication of mordenite zeolite does not significantly improve the catalytic efficiency of the mordenite zeolites.

With the deAl-mm-MOR/9 sample obtained by the removal of extraframework Al from mm-MOR/8 using oxalic acid, the formation of by-products at high temperatures was significantly reduced compared to mm-MOR/8 or microporous MOR/12 samples and was accompanied by a corresponding increase in the yield of the desired branched isomers, reaching a maximum of 67.4% at 275 °C. The deAl-mm-MOR/9 sample is characterised by shortened 12-ring channels due to well-developed secondary mesoporous structure, but without significantly enhanced accessibility of the OH groups compared to the parent zeolite (Table 2).

It seems that the shortening of the main channel and a larger number of channel openings provide only a slight increase in activity, but lead to a significant increase in selectivity limiting the non-selective subsequent cracking reactions and consequently increasing the yield of desired products at higher temperatures.

The deAl-mm-MOR/9.5 sample dealuminated by nitric acid provides higher yields of branched isomers compared to MOR/12 and mm-MOR/8 zeolites with similar yields of by-products (Figure 8). As the difference between deAl-mm-MOR/9.5 and deAl-mm-MOR/9 lies mainly in significantly higher accessibility of the OH groups (Table 2), the improvements in the yields of branched isomers at lower temperatures, e.g. from 53% to 67.7% at 250 °C, can be associated with greater accessibility of the acid sites, and the improvements in the yield at higher temperatures, e.g. from 58.7 to 67.4% at 275 °C, also with the shortened main channels and larger number of channel openings. Thus the use of the deAl-mm-MOR/9.5 sample had a positive effect on the yield of branched isomers in the whole temperature region. The improvements in the catalytic properties are minor, however, clearly indicating a potential for improvements in the functionality of hydroisomerization mordenite catalysts via enhanced accessibility of active sites and transport of reactants in the micro-mesoporous structure.

The durability and stability of the catalytic activity for the deAl-mm-MOR/9.5 as a representative micro-mesoporous Pt/H-MOR zeolite were analysed under the reaction conditions. Stable values of the yields of mono- and di-branched isomers ∼55% and ∼9%, respectively, and by-products ∼1% as a function of time-on-stream were obtained over deAl-mm-MOR/9.5 at 235 °C for 72 h indicating a sufficient structural stability and no deactivation of the micro-mesoporous Pt/H-MOR (Figure 9).

3.2.2 Hydroisomerization over partially dealuminated and acid-alkaline-acid treated mordenites

Figure 8C shows the yields of branched isomers as a function of temperature obtained over dealuminated deAl-MOR/16 and zeolites prepared by subsequent desilication and desilication/dealumination of the deAl-MOR/16 sample. Although the dealumination of mordenite (deAl-MOR/16) leads to a decrease in the concentration of Brønsted sites from 1.06 to 0.47 mmol.g^{-1}, the accessibility of the remaining acid sites was significantly enhanced, with ~ 92% Brønsted sites accessible for *n*-hexane (Table 2). Less than half the concentration of Brønsted sites in deAl-MOR/16 provided yields of branched hexanes which outperform the microporous MOR/12, cf. e.g. the yields of branched hexanes 36.5% and 54.1% at 225 °C for MOR/12 and deAl-MOR/16, respectively. The higher specific activity of acid-treated partially

dealuminated mordenites has been well documented in the literature [68] and explained by the beneficial effects on the textural properties of extraction of part of the framework Al atoms by acid treatment, leading to improved accessibility of highly active acid sites located in the 8-ring side pockets [5, 69]. Desilication of the deAl-MOR/16 sample yielded micro-mesoporous mm-deAl-MOR/9, which showed no significant changes in the yields of the branched isomers nor by-products. The positive impact of the development of the mesoporous volume (0.11 $cm^3.g^{-1}$) was probably offset by the negative impact of the decline in the microporous volume because of its partial blockage. The subsequent partial dealumination of mm-deAl-MOR/9 provided the deAl-mm-deAl-MOR/13 sample with well-developed mesoporous structure and with similar concentration and accessibility of the OH groups for n-hexane as the deAl-MOR/16 sample. The similar concentrations and accessibility of the OH groups for n-hexane in the deAl-MOR/16 and deAl-mm-deAl-MOR/13 samples resulted in similar yields of branched hexane isomers at ≤ 225 °C. The presence of mesoporous structures in deAl-mm-deAl-MOR/13 caused a slightly lower formation of cracking products and a corresponding increase in the yield of branched hexanes at higher temperatures ≥ 250 °C.

3.2.3 Hydroisomerization over fluorinated-alkaline treated mordenites

The yields of branched C_6 isomers in the hydroisomerization with microporous MOR/12 without postsynthesis treatment were very low at temperatures ≤ 200 °C. The yields were increased considerably over the mm-F-MOR/9.4 sample, e.g. from 13.5% to 47.2% at 200 °C, showing that the desilication of fluorinated mordenite zeolite markedly increased the catalytic activity (Figure 8E). This was accompanied by higher yields of di-branched isomers (Table 3) and high selectivity without the detectable formation of C_1-C_4 by-products at ≤ 200 °C (Figure 8F). In comparison with other micro-mesoporous Pt/H-MOR, the mm-F-MOR/9.4 sample provides the greatest enhancement of the yields of branched C_6 isomers achieved at low temperatures (Figure 10). The chemical analysis showed the absence of fluorine in the mm-F-MOR/9.4 treated after fluorination by desilication, triple ion-exchange with large excess of NH_4NO_3 solution and calcination in the air and subsequently in a hydrogen atmosphere. The enhancement in the activity is thus associated with the micro-mesoporous structure providing high concentration of Brønsted sites (c_B 0.6 mmol.g^{-1}) readily accessible for n-hexane molecules (> 90%), (Table 2). To exclude a possible effect of traces of fluoride not detectable by the chemical analysis on the increase in activity, a fluorinated sample of Pt/H-F-ZSM-5 zeolite with small crystals was prepared and its activity was compared with Pt/H-ZSM-5. The intra-crystalline diffusion does not affect the overall reaction rates for ZSM-5 for both the n-

hexane hydroisomerization [61] and cracking [70]. Accordingly, we observed very comparable yields of branched C_6 isomers over Pt/H-ZSM-5 and its fluorinated analogue Pt/H-F-ZSM-5 in the entire temperature region (Figure S9). Thus, the high concentration of the Brønsted sites located in non-restricted micropores highly accessible via new channel openings in small mesopores formed by the simultaneous removal of Si and Al atoms results in significantly improved catalytic properties enabling the reaction at lower temperatures.

4. Discussions

4.1 Structure of micro-mesoporous mordenites obtained by leaching methods

Selective dissolution of silicon-rich areas of the framework and the extraction of aluminum are inherent parts of the acid and alkali treatments of zeolites, respectively. Our results clearly show that, for the formation of micro-mesoporous mordenite with Brønsted active sites readily accessible in non-restricted micropores, it is necessary to extract both silicon and aluminum atoms in a controlled way ensuring the formation of mesopores and preservation of micropores and the majority of the framework Al. Particularly for desilication of mordenites with a high concentration of aluminum in the framework (Si/Al ~ 12), the extraframework tetrahedrally coordinated $AlO_x/(OH)_y$ species, formed by hydrolysis and dislodgment of a small fraction of framework Al, block a significant part of the pseudo-monodimensional 12-ring channels and/or accessibility of the acid sites in 8-ring side pockets. Desilication of mordenite surprisingly does not lead to greater accessibility of the acid sites; to the contrary, a significant part of the micropores is diffusion-limited even for nitrogen molecules. However, subsequent acid leaching under specific conditions, characterized by a low concentration of oxalic or nitric acid, leads to efficient removal of the extra-framework and/or perturbed framework Al species formed in mesopores after desilication and blocking part of the micropores. The concentration of the Brønsted sites determined by d_3-acetonitrile and their accessibility for *n*-hexane as a relevant molecular probe for the hydroisomerization reaction indicate that the prevailing amount of the framework Al atoms is not dislodged during either the dissolution of silicon-rich areas of the framework or the selective extraction of the extraframework Al. Thus the alkaline removal of parts of the Si-rich framework and subsequent selective acid leaching of extraframework Al and only small amount of framework Al resulted in a micro-mesoporous mordenite structure with high concentration of strongly acidic Brønsted sites readily accessible in both 12-ring and 8-ring channels. The desilication with subsequent removal of only extraframework Al creates a number of new channel openings in mesopores effectively shortening of the main 12-ring channels. However, the dealumination of a small fraction of the

framework Al atoms is indispensable for significant enhancement of the accessibility of the OH groups in 8-ring side pockets. It should be also mentioned that the increase in the concentration of Lewis centres and an intense signal of internal Si-OH groups suggests that the massive changes in the texture of the zeolite towards a well-developed mesoporous structure leads to the disruption of part of the regularly arranged atoms originally present in the low-defective zeolitic structure.

The alkaline leaching of mordenite pre-impregnated with a solution of NH_4F appeared to be the most efficient approach for creating the secondary mesoporous structure in mordenite zeolite with a high concentration of readily accessible Brønsted sites. This procedure enabled controlled extraction of Si atoms and concomitantly the framework F-bearing tetrahedral Al species. The dissolution of tetrahedrally coordinated $Al(FO_3)$ and SiO_4 entities during alkaline treatment resulted in secondary mesoporosity and opened non-restricted channel openings of the preserved microporous structure with high concentration of Brønsted sites readily accessible for *n*-hexane. A difference was observed in the modes of formation and types of mesoporous structures obtained by desilication-acid treatment and desilication of fluorinated mordenite. With desilication-acid treatment, circular mesopores 5-20 nm in size were predominant while desilication of fluorinated mordenite yielded small mesopores combined with mesopores formed along crystal boundaries and intergrowths.

4.2 Effect of micro-mesoporous structure on hydroisomerization of n-hexane

The molecules involved in hydroisomerization either as reactants or products have similar sizes to those of the mordenite pores (Figure 1) [14]. Consequently, the access of these molecules to active sites is a key factor governing the performance of mordenite catalysts. The most obvious effects of the introduction of secondary mesoporosity on the yields of branched hexanes obtained in this study is illustrated at Figure 10. Whereas only a small increase in the yield of branched isomers from 13.5% to 16% was obtained after dealumination, the increase in the yield to 22% was appreciable with concurrent introduction of mesoporous structure by desilication and partial dealumination; note that, at a temperature of 200 °C, the reaction exhibits > 99% selectivity for branched isomers and the formation of C_1-C_5 by-products practically did not proceed over any of the analysed catalysts (Figure 8). The sole partial dealumination significantly improved the accessibility of the OH groups (~ 90%) in the mordenite channels, but the benefit was to a significant extent offset by a significant decrease in their concentration. The introduction of mesoporous structure via subsequent desilication by alkaline treatment and partial dealumination by diluted acid can yield a similar percentage of

accessible OH groups to dealumination, but with their slightly higher concentrations. Desilication alone yielded mesopores 5-20 nm in size and does not lead to significant exposure of the OH groups to the reactant molecules and subsequent partial dealumination is also a necessary step in obtaining highly accessible OH groups. This necessarily leads to a reduction in the concentration of OH groups and limits their maximum available concentration. The high accessibility of acid sites in micro-mesoporous mordenite obtained by sequential alkaline and mild acid treatments is connected with catalytic performance exceeding that of microporous mordenite; however the improvements in the yields are slight. To attain more significant improvement in the activities, a mordenite structure characterised by a higher concentration of Brønsted sites readily accessible for C_6 molecules is crucial. A micro-mesoporous structure characterised by small mesopores and a high concentration of well accessible acid sites was obtained by desilication of fluorinated mordenite zeolite. This treatment results in markedly improved catalyst activity and a large increase in the yield of branched isomers (Figures 8 and 10). Thus it is clear that the micro-mesoporous structure with high density of readily accessible OH groups is ultimately connected with catalytic properties greatly exceeding those of microporous or partially dealuminated mordenite zeolite. The concentrations of accessible Brønsted sites were correlated with the activity measured for all the micro-mesoporous Pt/H-MOR zeolites (Figure 11). The yields of branched C_6 isomers clearly increase with the concentrations of the Brønsted sites accessible for *n*-hexane molecule. We also analysed the relationships between the concentrations of the Brønsted sites in 8-rings or 12-rings estimated using analysis of the FTIR absorption bands of the bridging OH groups in zeolites (Figure S5), and the hydroisomerization activity (Figure S10). The plots of the yields of branched C_6 isomers against the concentrations of the Brønsted sites in 8-ring or 12-ring channels did not show any direct relationship. According to the Chiang et al. [8], the higher activity of the protonic sites in the 8-ring pockets of H-MOR is associated with a specific deformation and partial confinement of the C_6 molecule in the 8-ring. In the case of MOR zeolites with hierarchical porosity, the local structure and mainly the openings of the 8-ring pockets are largely affected (see Figure 6) and the specific activity of corresponding protonic sites could be altered.

Summing up, the analysis of the hydroisomerization over micro-mesoporous Pt/H-MOR zeolites exhibiting quite different levels of hierarchical structure and the overall concentrations of acid sites, and thus the different concentrations of accessible Brønsted sites, shows that the hierarchical porosity has promotional effect on activity of acid sites even for the relatively small C_6 molecules. The increase in the yields of branched isomers over the micro-mesoporous structure with a high concentration of readily accessible Brønsted sites enables a shift of the

operation window to lower temperatures with more favourable thermodynamic equilibrium for branched isomers.

Conclusions

The critical function of the micro-mesoporous structure and the concentration and accessibility of Brønsted sites for hydroisomerization of linear hexane was elucidated by using three series of micro-mesoporous mordenite zeolites differing in their mesoporosity and concentration and the accessibility of acid sites. The hydroisomerization of *n*-hexane over microporous Pt/H-mordenite is limited by mass transfer effects due to the low accessibility of acid sites in 8-ring channels and the diffusion-restricted pseudo-monodimensional channel structure. The introduction of secondary mesoporosity into mordenite using the alkaline-acid, acid-alkaline-acid, and fluorination-alkaline postsynthesis treatments proposed in this study effectively shortens the length of the 12-ring main channels, opens the side 8-ring channel-pockets, provides the high concentration of Brønsted sites and enhances the accessibility of the acid sites for hexane molecules. The shortening of the main 12-ring channels and a larger number of channel openings provide an increase in the selectivity, limiting the nonselective subsequent cracking reactions and consequently increasing the yield of the desired products at higher temperatures. The micro-mesoporous mordenite structure with the Brønsted sites in the environment of the micropores and accessible through mesopores alleviates the diffusion limitations due to restricted access and slow transport to/from the active site, resulting in a significant increase in the catalyst efficiency and improvements in the selectivity in skeletal hydroisomerization of *n*-hexane into branched isomers. It enables efficient isomerization in a temperature region that is thermodynamically more favourable for desired di-branched isomers.

Supporting Information

Description of the structure of parent mordenite zeolite, SEM images, X-ray diffraction patterns, nitrogen adsorption and desorption in a log P scale, and ^{27}Al MAS NMR spectra for the micro-mesoporous mordenite zeolites, an illustration of analysis of the FTIR absorption bands of the bridging OH groups of dehydrated zeolites and the C≡N groups of adsorbed d_3-acetonitrile, an illustration of analysis of the OH groups accessibility using FTIR spectra of adsorbed *n*-hexane, TEM images and FTIR spectra of CO adsorbed on the reduced microporous and micro-mesoporous Pt/H-MOR, and some supplementary kinetic data are available in the Supporting Information.

Acknowledgments

References

1.	Iglesia, E.; Soled, S. L.; Kramer, G. M. *J. Catal.* **1993**, *144*, 238-253.
2.	Iglesia, E.; Barton, D. G.; Soled, S. L.; Miseo, S.; Baumgartner, J. E.; Gates, W. E.; Fuentes, G. A.; Meitzner, G. D., Selective isomerization of alkanes on supported tungsten oxide acids. In *Stud. Surf. Sci. Catal*, **1996**, *101A*, 533-542.
3.	Chica, A.; Corma, A. *J. Catal.* **1999**, *187*, 167-176.
4.	Ono, Y. *Catal. Today* **2003**, *81*, 3-16.
5.	Tromp, M.; van Bokhoven, J. A.; Garriga Oostenbrink, M. T.; Bitter, J. H.; de Jong, K. P.; Koningsberger, D. C. *J. Catal.* **2000**, *190*, 209-214.
6.	Gounder, R.; Iglesia, E. *Angew. Chem., Int. Ed.* **2010**, *49*, 808-811.
7.	Bhan, A.; Iglesia, E. *Acc. Chem. Res.* **2008**, *41*, 559-567.
8.	Chiang, H.; Bhan, A. *J. Catal.* **2011**, *283*, 98-107.
9.	Van Laak, A. N. C.; Sagala, S. L.; Zecevic, J.; Friedrich, H.; De Jongh, P. E.; De Jong, K. P. *J. Catal.* **2010**, *276*, 170-180.
10.	Centi, G.; Perathoner, S. *Coord. Chem. Rev.* **2011**, *255*, 1480-1498.
11.	Groen, J. C.; Zhu, W.; Brouwer, S.; Huynink, S. J.; Kapteijn, F.; Moulijn, J. A.; Pérez-Ramírez, J. *J. Am. Chem. Soc.* **2007**, *129*, 355-360.
12.	Gobin, O. C.; Reitmeier, S. J.; Jentys, A.; Lercher, J. A. *J. Phys. Chem. C* **2011**, *115*, 1171-1179.
13.	Park, D. H.; Kim, S. S.; Wang, H.; Pinnavaia, T. J.; Papapetrou, M. C.; Lappas, A. A.; Triantafyllidis, K. S. *Angew. Chem.* **2009**, *48*, 7645-7648.
14.	Ferreira, A. F. P.; Mittelmeijer-Hazeleger, M. C.; Granato, M. A.; Martins, V. F. D.; Rodrigues, A. E.; Rothenberg, G. *Phys. Chem. Chem. Phys.* **2013**, *15*, 8795-8804.
15.	Fan, W.; Snyder, M. A.; Kumar, S.; Lee, P. S.; Yoo, W. C.; McCormick, A. V.; Lee Penn, R.; Stein, A.; Tsapatsis, M. *Nature Mater.* **2008**, *7*, 984-991.
16.	Hartmann, M. *Angew. Chem., Int. Ed.* **2004**, *43*, 5880-5882.
17.	Inayat, A.; Knoke, I.; Spiecker, E.; Schwieger, W. *Angew. Chem., Int. Ed.* **2012**, *51*, 1962-1965.

18.	Perez-Ramirez, J. *Nat. Chem.* **2012**, *4*, 250-251.
19.	Sazama, P.; Sobalik, Z.; Dedecek, J.; Jakubec, I.; Parvulescu, V.; Bastl, Z.; Rathousky, J.; Jirglova, H. *Angew. Chem., Int. Ed.* **2013**, *52*, 2038-2041.
20.	Sun, J. L.; Bonneau, C.; Cantin, A.; Corma, A.; Diaz-Cabanas, M. J.; Moliner, M.; Zhang, D. L.; Li, M. R.; Zou, X. D. *Nature* **2009**, *458*, 1154-1157.
21.	Choi, M.; Na, K.; Kim, J.; Sakamoto, Y.; Terasaki, O.; Ryoo, R. *Nature* **2009**, *461*, 246-249.
22.	Zhang, X. Y.; Liu, D. X.; Xu, D. D.; Asahina, S.; Cychosz, K. A.; Agrawal, K. V.; Al Wahedi, Y.; Bhan, A.; Al Hashimi, S.; Terasaki, O.; Thommes, M.; Tsapatsis, M. *Science* **2012**, *336*, 1684-1687.
23.	Jacobsen, C. J. H.; Madsen, C.; Houzvicka, J.; Schmidt, I.; Carlsson, A. *J. Am. Chem. Soc.* **2000**, *122*, 7116-7117.
24.	De Jong, K. P.; Zecevic, J.; Friedrich, H.; De Jongh, P. E.; Bulut, M.; Van Donk, S.; Kenmogne, R.; Finiels, A.; Hulea, V.; Fajula, F. *Angew. Chem. Int. Ed.* **2010**, *49*, 10074-10078.
25.	Groen, J. C.; Moulijn, J. A.; Perez-Ramirez, J. *J. Mater. Chem.* **2006**, *16*, 2121-2131.
26.	Góra-Marek, K.; Tarach, K.; Tekla, J.; Olejniczak, Z.; Kuśtrowski, P.; Liu, L.; Martinez-Triguero, J.; Rey, F. *J. Phys. Chem. C* **2014**, *118*, 28043-28054.

27.	Paixao, V.; Carvalho, A. P.; Rocha, J.; Fernandes, A.; Martins, A. *Microporous Mesoporous Mat.* **2010**, *131*, 350-357.

28.	Wichterlova, B.; Tvaruzkova, Z.; Sobalik, Z.; Sarv, P. *Microporous Mesoporous Mater.* **1998**, *24*, 223-233.

29.	Fyfe, C. A.; Feng, Y.; Grondey, H.; Kokotailo, G. T.; Gies, H. *Chem. Rev. (Washington, DC, U. S.)* **1991**, *91*, 1525-1543.

30.	Engelhardt, G.; Lohse, U.; Lippmaa, E.; Tarmak, M.; Magi, M. *Z. Anorg. Allg. Chem.* **1981**, *482*, 49-64.

31.	Eder, F.; Stockenhuber, M.; Lercher, J. A. *J. Phys. Chem. B* **1997**, *101*, 5414-5419.

32.	Zholobenko, V. L.; Makarova, M. A.; Dwyer, J. *J. Phys. Chem.* **1993**, *97*, 5962-5964.

33.	Bordiga, S.; Lamberti, C.; Geobaldo, F.; Zecchina, A.; Palomino, G. T.; Arean, C. O. *Langmuir* **1995**, *11*, 527-533.

34.	Wakabayashi, F.; Kondo, J.; Wada, A.; Domen, K.; Hirose, C. *J. Phys. Chem.* **1993**, *97*, 10761-10768.

35.	Alberti, A. *Zeolites* **1997**, *19*, 411-415.

36.	Eder, F.; Stockenhuber, M.; Lercher, J. A. *J. Phys. Chem. B* **1997**, *101*, 5414-5419.

37.	Viswanadham, N.; Kumar, M. *Microporous Mesoporous Mat.* **2006**, *92*, 31-37.

38.	Lietz, G.; Schnabel, K. H.; Peuker, C.; Gross, T.; Storek, W.; Volter, J. *J. Catal.* **1994**, *148*, 562-568.

39.	Remy, M. J.; Stanica, D.; Poncelet, G.; Feijen, E. J. P.; Grobet, P. J.; Martens, J. A.; Jacobs, P. A. *J. Phys. Chem.* **1996**, *100*, 12440-12447.

40.	Chen, T. H.; Wouters, B.; Grobet, P. *Chem. J. Internet* **2000**, *2*, 7-13.

41.	Chen, T. H.; Wouters, B. H.; Grobet, P. J. *Eur. J. Inorg. Chem.* **2000**, 281-285.

42.	Wouters, B. H.; Chen, T.; Grobet, P. J. *Journal of Physical Chemistry B* **2001**, *105*, 1135-1139.

43.	Chen, J.; Chen, T.; Guan, N.; Wang, J. *Catal. Today* **2004**, *93-95*, 627-630.

44.	Samoson, A.; Lippmaa, E.; Engelhardt, G.; Lohse, U.; Jerschkewitz, H. G. *Chem. Phys. Lett.* **1987**, *134*, 589-592.

45.	Sazama, P.; Wichterlova, B.; Dedecek, J.; Tvaruzkova, Z.; Musilova, Z.; Palumbo, L.; Sklenak, S.; Gonsiorova, O. *Microporous Mesoporous Mat.* **2011**, *143*, 87-96.

46.	Sayed, M. B.; Kydd, R. A.; Cooney, R. P. *J. Catal.* **1984**, *88*, 137-149.

47.	Kustov, L. M.; Kazansky, V. B.; Beran, S.; Kubelkova, L.; Jiru, P. *J. Phys. Chem.* **1987**, *91*, 5247-5251.

48.	Fritz, P. O.; Lunsford, J. H. *J. Catal.* **1989**, *118*, 85-98.

49.	Groen, J. C.; Jansen, J. C.; Moulijn, J. A.; Pérez-Ramírez, J. *J. Phys. Chem. B* **2004**, *108*, 13062-13065.

50.	Svelle, S.; Sommer, L.; Barbera, K.; Vennestrøm, P. N. R.; Olsbye, U.; Lillerud, K. P.; Bordiga, S.; Pan, Y. H.; Beato, P. *Catal. Today* **2011**, *168*, 38-47.

51.	Giudici, R.; Kouwenhoven, H. W.; Prins, R. *Appl. Catal., A* **2000**, *203*, 101-110.

52.	Van Geem, P. C.; Scholle, K. F. M. G. J.; Van Der Velden, G. P. M.; Veeman, W. S. *J. Phys. Chem.* **1988**, *92*, 1585-1589.

53.	Muller, M.; Harvey, G.; Prins, R. *Microporous Mesoporous Mat.* **2000**, *34*, 135-147.

54.	Silaghi, M.-C.; Chizallet, C.; Sauer, J.; Raybaud, P. *J. Catal.* **2016**, *339*, 242-255.

55.	Yu, L.; Huang, S.; Miao, S.; Chen, F.; Zhang, S.; Liu, Z.; Xie, S.; Xu, L. *Chem. Eur. J.* **2015**, *21*, 1048-1054.

56.	Qin, Z.; Lakiss, L.; Gilson, J. P.; Thomas, K.; Goupil, J. M.; Fernandez, C.; Valtchev, V. *Chem. Mater.* **2013**, *25*, 2759-2766.

57.	Pérez-Ramírez, J.; Christensen, C. H.; Egeblad, K.; Christensen, C. H.; Groen, J. C. *Chem. Soc. Rev.* **2008**, *37*, 2530-2542.

58.	Milina, M.; Mitchell, S.; Crivelli, P.; Cooke, D.; Pérez-Ramírez, J. *Nat. Commun.* **2014**, *5*, 3922.

59.	Reitmeier, S. J.; Gobin, O. C.; Jentys, A.; Lercher, J. A. *Angew. Chem., Int. Ed.* **2009**, *48*, 533-538.

60.	Ribeiro, F.; Marcilly, C.; Guisnet, M. *J. Catal.* **1982**, *78*, 267-274.

61.	Van De Runstraat, A.; Kamp, J. A.; Stobbelaar, P. J.; Van Grondelle, J.; Krijnen, S.; Van Santen, R. A. *J. Catal.* **1997**, *171*, 77-84.

62. Stakheev, A. Y.; Shpiro, E. S.; Tkachenko, O. P.; Jaeger, N. I.; Schulz-Ekloff, G. *J. Catal.* **1997**, *169*, 382-388.

63. Kubanek, P.; Schmidt, H. W.; Spliethoff, B.; Schüth, F. *Microporous Mesoporous Mat.* **2005**, *77*, 89-96.

64. Monteiro, R.; Ania, C. O.; Rocha, J.; Carvalho, A. P.; Martins, A. *Appl. Catal., A.* **2014**, *476*, 148-157.

65. Zecevic, J.; Vanbutsele, G.; De Jong, K. P.; Martens, J. A. *Nature* **2015**, *528*, 245-254.

66. Sazama, P.; Kaucky, D.; Moravkova, J.; Pilar, R.; Klein, P.; Pastvova, J.; Tabor, E.; Sklenak, S.; Jakubec, I.; Mokrzycki, L. *Appl Catal A Gen* **2017**, *533*, 28-37.

67. Monteiro, R.; Ania, C. O.; Rocha, J.; Carvalho, A. P.; Martins, A. *Applied Catalysis A: General* **2014**, *476*, 148-157.

68. Leng, K.; Wang, Y.; Hou, C.; Lancelot, C.; Lamonier, C.; Rives, A.; Sun, Y. *J. Catal.* **2013**, *306*, 100-108.

69. Nesterenko, N. S.; Thibault-Starzyk, F.; Montouillout, V.; Yuschenko, V. V.; Fernandez, C.; Gilson, J. P.; Fajula, F.; Ivanova, I. I. *Microporous Mesoporous Mater.* **2004**, *71*, 157-166.

70. Haag, W. O.; Lago, R. M.; Weisz, P. B. *Faraday Discuss. Chem. Soc.* **1981**, *72*, 317-330.

Table 1. Preparation and textural properties of micro-mesoporous mordenite zeolites.

Sample	Preparation	Si/Al[a]	Si/Al$_{FR}$[b]	V_{tot} (P/P$_0$~0.8) (cm^3. g^{-1})	V_{MI}[c]	V_{MESO}[d]	S_{EXT}[c] (m^2. g^{-1})
MOR/12	Microporous parent MOR	12.1	12.5	0.24	0.19	0.05	42
mm-MOR/8	+0.2M NaOH	8.7	10.2	0.14	0.06	0.08	79
deAl-mm-MOR/9	+0.2M NaOH+0.1M (COOH)$_2$	9	11.2	0.24	0.13	0.11	107
deAl-mm-MOR/9.5	+0.2M NaOH+0.1M HNO$_3$	9.5	-	0.25	0.13	0.12	114
deAl-MOR/16	+3M HNO$_3$	16.1	-	0.24	0.19	0.05	44
mm-deAl-MOR/9.1	+3M HNO$_3$+0.2M NaOH	9.1	-	0.26	0.15	0.11	102
deAl-mm-deAl-MOR/13	+3M HNO$_3$+0.2M NaOH+0.1M HNO$_3$	13.5	-	0.26	0.19	0.09	88
deAl-mm-deAl-MOR/30	+3M HNO$_3$+0.2M NaOH+0.1M (COOH)$_2$	30	-	0.30	0.20	0.10	95
mm-F-MOR/9.4	+ 0.36 M NH$_4$F + 0.2M NaOH	9.4	-	0.23	0.14	0.09	104
deAl-mm-F-MOR/13.6	+ 0.36 M NH$_4$F+0.2M NaOH+0.1M HNO$_3$	13.6	-	0.22	0.14	0.08	104

[a] from chemical analysis

[b] from ^{29}Si MAS NMR

[c] estimated from the BdB *t-plot*

[d] $V_{meso} = V_{total} - V_{micro}$

Table 2. The concentrations of Brønsted and Lewis sites and the accessibility of OH groups in micro-mesoporous mordenites.

Sample	Si/Al[a]	c_{Al}[a]	c_B[b]	c_L[c]	c_{B+2L}[d]	Accessibility of OH groups[e] (%)
			(mmol.g^{-1})			
MOR/12	12.1	1.23	1.06	0.12	1.30	64.1
mm-MOR/8	8.7	1.49	0.44	0.14	0.72	-
deAl-mm-MOR/9	9	1.67	0.81	0.35	1.51	68.7
deAl-mm-MOR/9.5	9.5	1.60	0.55	0.20	0.95	79.1
deAl-MOR/16	16.1	0.97	0.47	0.13	0.73	92.6
mm-deAl-MOR/9.1	9.1	1.65	0.44	0.22	0.88	-
deAl-mm-deAl-MOR/13	13.5	1.15	0.43	0.45	1.33	91.6
deAl-mm-deAl-MOR/30	30	0.53	0.27	0.20	0.67	74.4
mm-F-MOR/9.4	9.4	1.61	0.60	0.24	1.09	90.0

[a] from chemical analysis

[b, c] concentrations of acid Brønsted and Lewis sites, respectively, from the FTIR spectra of adsorbed d_3-acetonitrile

[d] concentration of Al estimated from the concentration of Brønsted and Lewis sites ($c_{Al} = c_B + 2c_L$)

[e] from the FTIR spectra of the bridging OH groups after adsorption of n-hexane

Table 3. The yields of branched hexane isomers and lower molecular weight by-products for hydroisomerization of *n*-hexane over microporous and micro-mesoporous Pt/H-MOR at 225 °C and 250 °C.

Sample	Σy_{iso-C6} (%)		2,2-dimethyl-		2,3-dimethyl-		2-methyl-		3-methyl-		C_1-C_5 (%)	
	225 °C	250 °C	225 °C	250 °C	225 °C	250 °C	225 °C	250 °C	225 °C	250 °C	225 °C	250 °C
Pt/H-MOR/12	36.5	53.0	1.6	3.6	6.0	6.0	7.3	8.4	21.6	35	0.5	5.3
Pt/H-mm-MOR/8	40.1	59.2	2.5	5.2	5.2	6.3	7.9	8.6	24.5	39.1	0.9	7.5
Pt/H-deAl-mm-MOR/9	37.5	61.9	2.1	5.4	4.7	6.7	8.7	8.7	22.0	41.1	0.6	4.1
Pt/H-deAl-mm-MOR/9.5	48.7	67.7	1.8	5.7	6.1	7.3	8.8	10.5	32.0	44.2	3.0	7.6
Pt/H-deAl-MOR/16	54.1	60.8	2.9	4.9	6.1	6.8	11.2	11.3	33.9	37.8	3.9	16
Pt/H-mm-deAl-MOR/9.1	45.8	63.4	2.8	8.1	4.5	6.5	8.6	8.6	29.9	40.2	2.9	10.4
Pt/H-deAl-mm-deAl-MOR/13	50.0	67.5	2.4	6.3	5.0	7.4	8.2	10.0	34.4	43.8	3.7	8.7
Pt/H-deAl-mm-deAl-MOR/30	23.7	47.9	0.6	3.5	1.3	4.2	7.3	8.4	14.5	31.8	5.0	12.4
Pt/H-mm-F-MOR/9.4	62.5	59.6	4.9	7.4	7.4	6.2	8.6	8.4	41.6	37.6	6.4	18.5
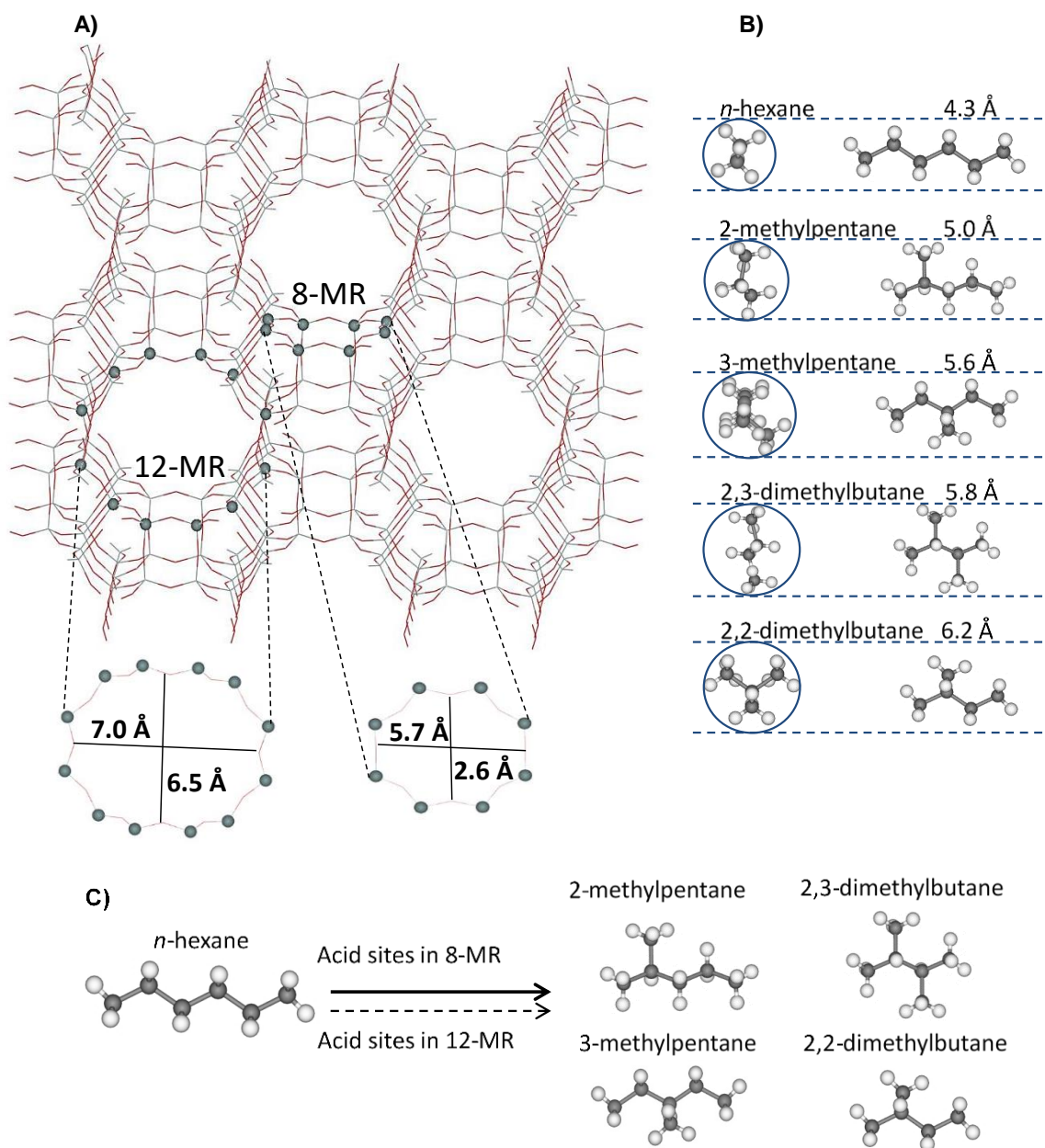
Figure 1. Illustration of the size-restriction of 8-ring compared to 12-ring channels in skeletal isomerization of *n*-hexane over mordenite zeolite. A) Topology of microporous mordenite zeolite consisting 12-ring (7.0 Å x 6.5 Å) channel and 8-ring (5.7 Å x 2.6 Å) side-pockets, B) kinetic diameters of hexane isomers [12], and C) the reaction scheme.
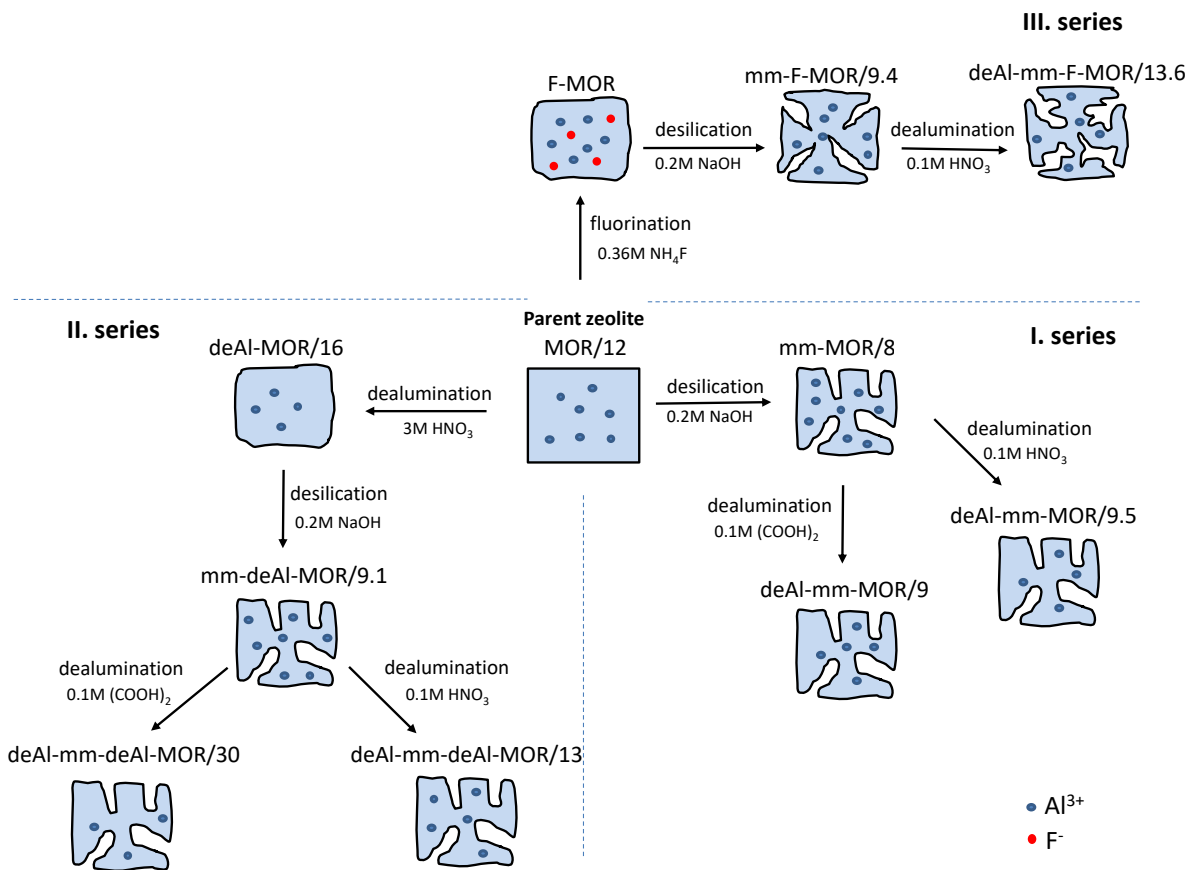
Figure 2. Schema of the preparation of micro-mesoporous mordenite zeolites using postsynthesis alkaline-acid (Series I), acid-alkaline-acid (Series II), and fluorination-alkaline-acid (Series III) leaching procedures.
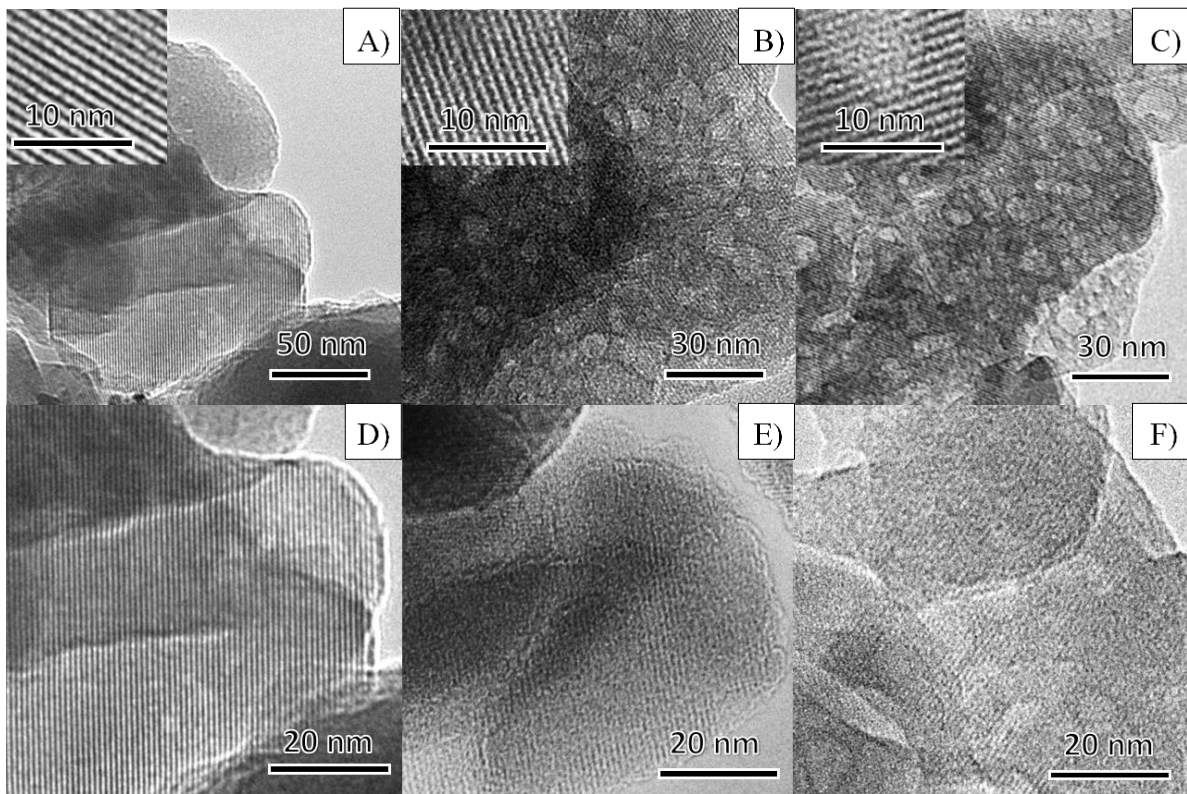
Figure 3. Represetative HR-TEM images of A) and D) microporous MOR (MOR/12), B) micro-mesoporous MOR (mm-MOR/8), C) dealuminated micro-mesoporous (deAl-mm-MOR/9.5), E) fluorinated MOR (F-MOR), and F) fluorinated micro-mesoporous MOR (mm-F-MOR/9.4).
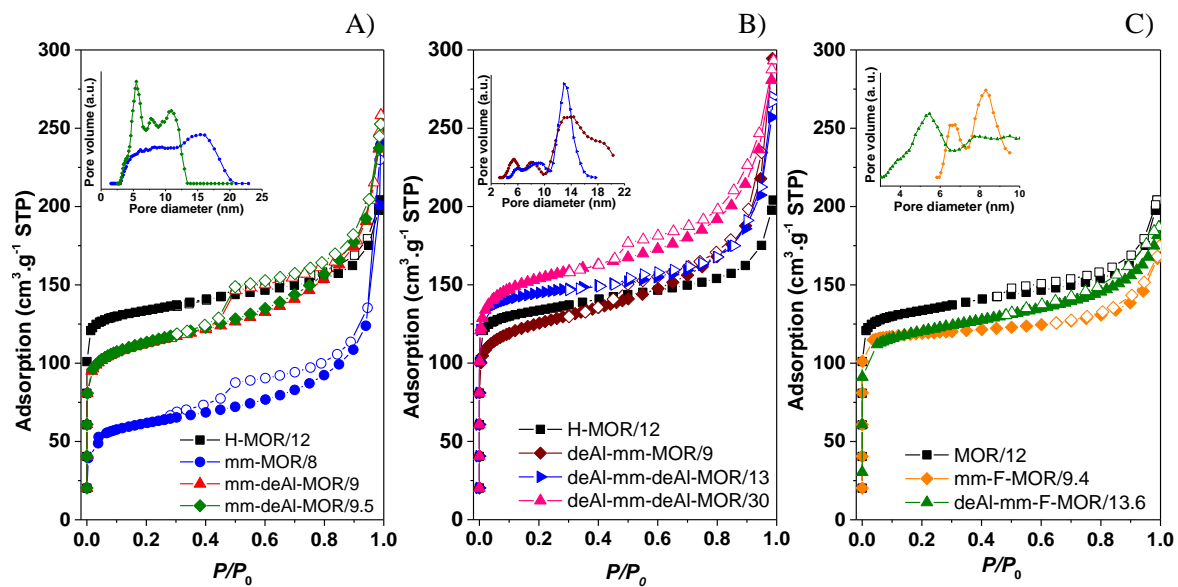
Figure 4. Nitrogen adsorption (solid symbols) and desorption (open symbols) at 77 K on microporous and micro-mesoporous mordenite zeolites prepared by sequential alkaline and acid leaching for A) Series I., B) Series II., C) Series III.
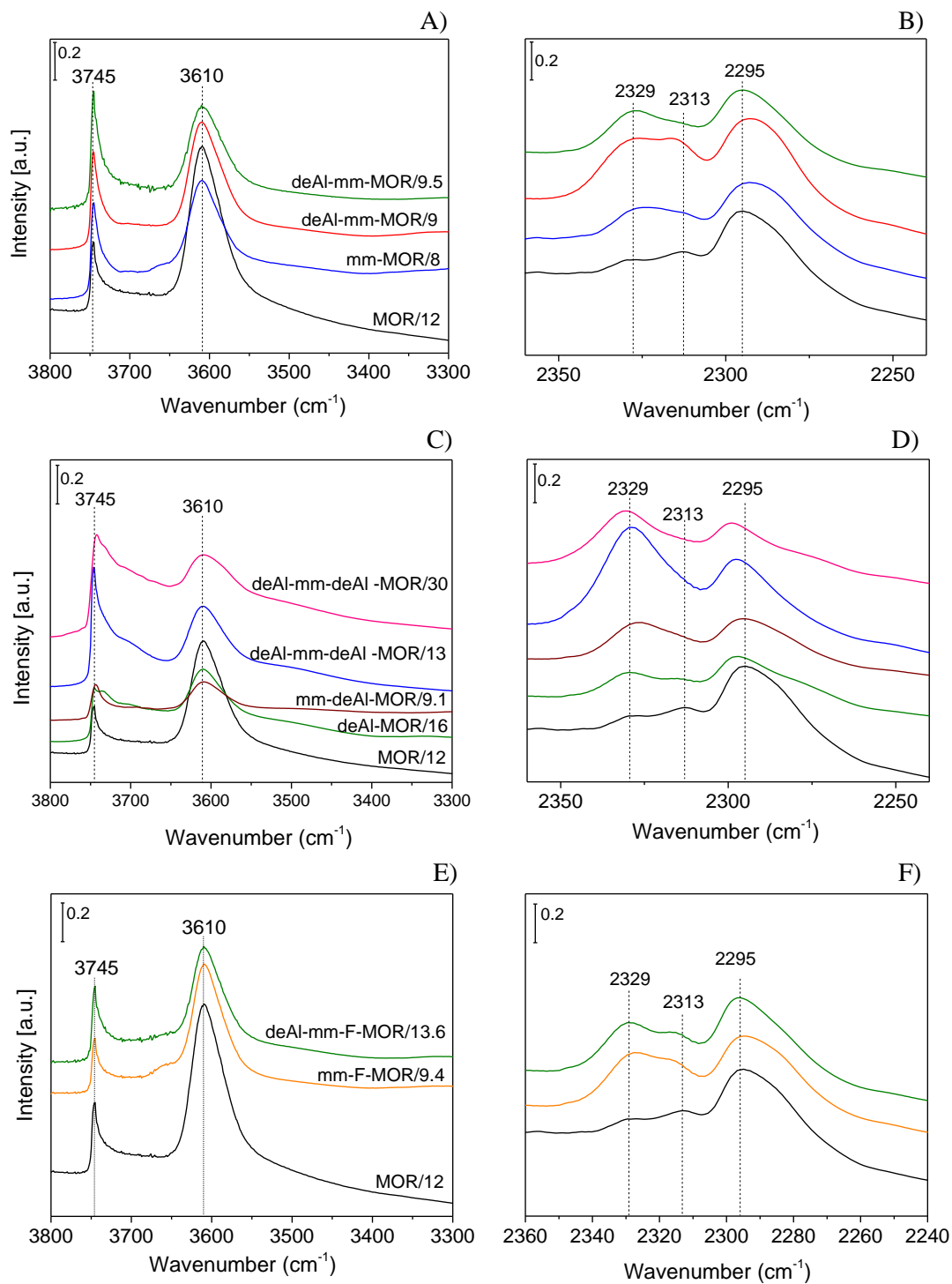
Figure 5. FTIR spectra of adsorbed d_3-acetonitrile (B, D, and F) and FTIR spectra in the OH stretching region (A, C, and F) for microporous and micro-mesoporous H-MOR zeolites. A, B) Series I.; C, D) Series II.; and E, F) Series III.
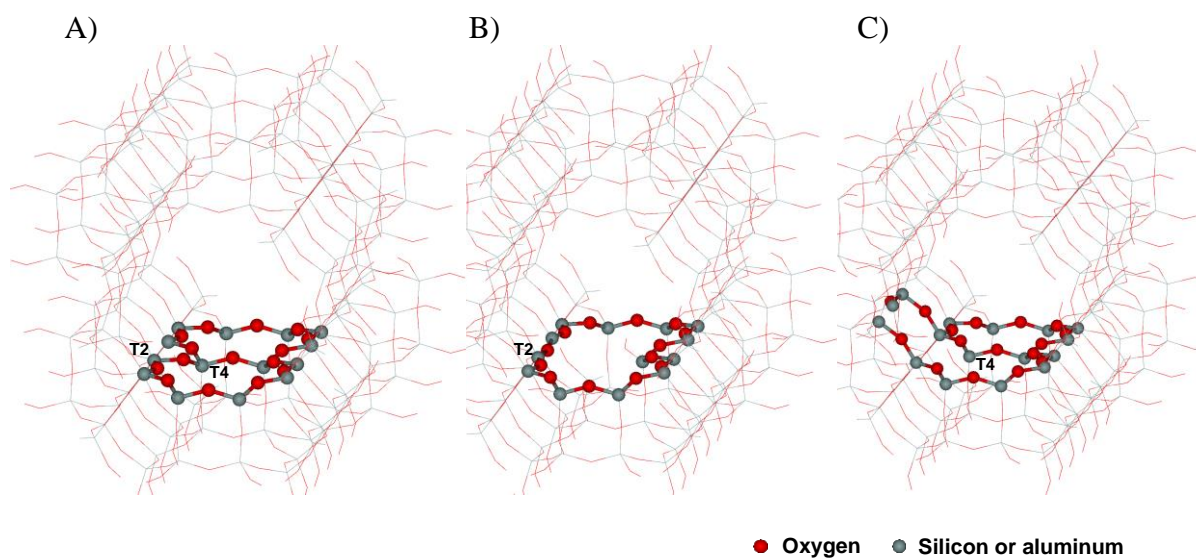
Figure 6. Schematic illustration of the effect of the extraction of one T atom from 8-ring on the local structure of the openings of the side-pockets in MOR zeolite. A) Two neighbouring 8-rings and the same structure with removed B) T4 atom and C) T2 atom.
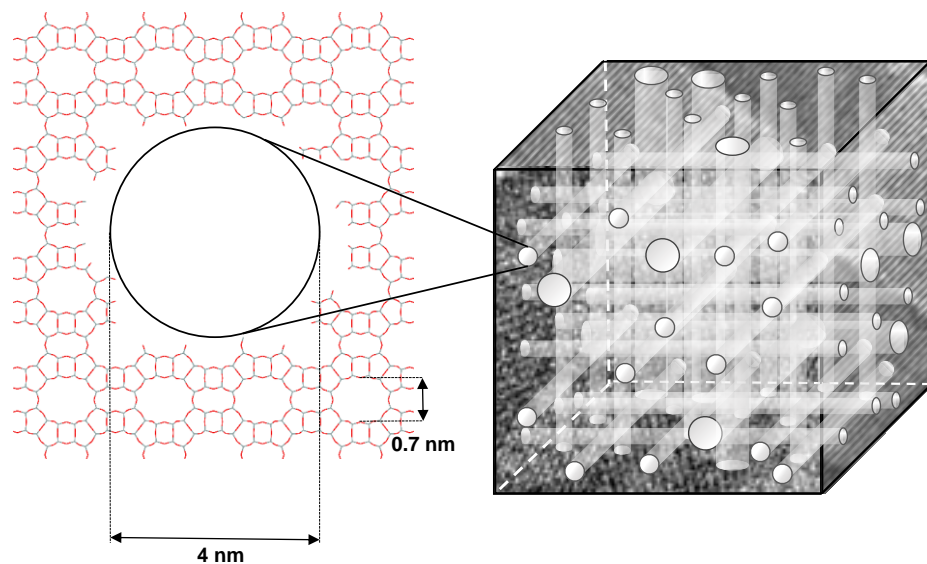
The length of the channels in the mordenite (crystal size 80 nm).

Structure	Mesopore diameter (nm)	Max. diffusion path in channels (nm)
Microporous	-	80
Micro-mesoporous $V_{MESO} = 0.09$ cm³.g⁻¹	8	42
	4	39
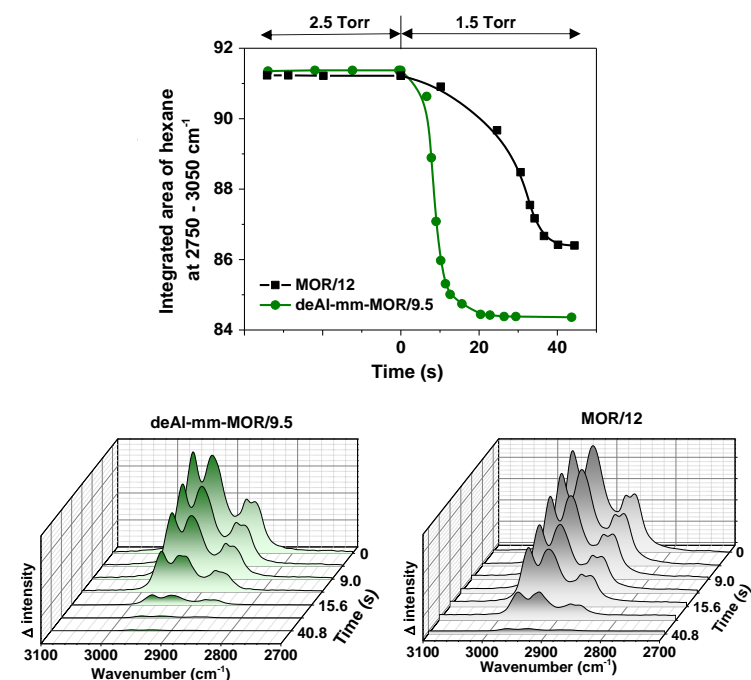
Figure 7. Analysis of the effect of the presence of mesopores on the length of zeolite channels and diffusion of *n*-hexane: A) Model determining the length of diffusion path through the mordenite channel, where 4 and 8 nm channels oriented along the axes and internal mesopore volume 0.09 cm³.g⁻¹ were considered. B) Desorption of *n*-hexane initiated by changes in the *n*-hexane partial pressure from 2.5 to 1.5 Torr analysed by FTIR spectroscopy.
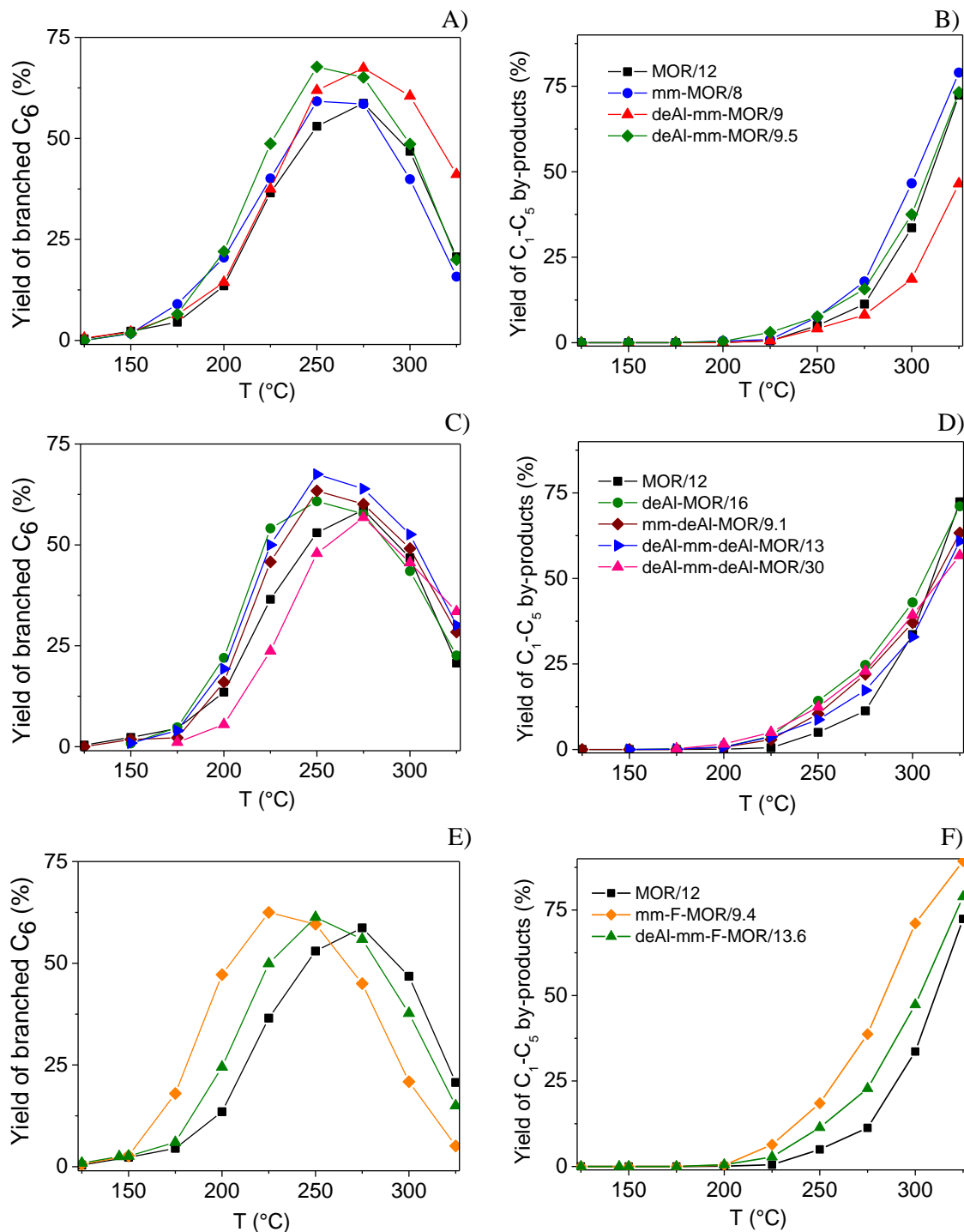
Figure 8. The yields of branched C_6 isomers and C_1-C_5 by-products in the hydroisomerization of *n*-hexane over Pt/H-MOR zeolites as a function of temperature. A, B) Series I.; C, D) Series II.; and E, F) Series III.
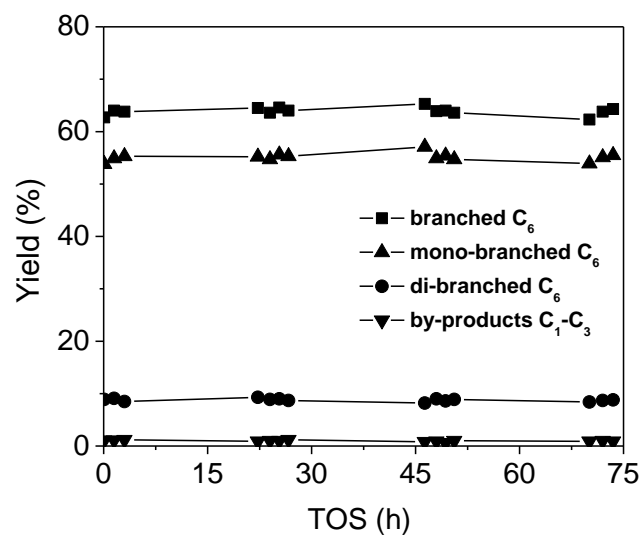
Figure 9. Dependence of the yield of branched hexane isomers and C_1-C_3 by-products on time-on-stream (TOS) in hydroisomerization of *n*-hexane over Pt/H-deAl-mm-MOR/9.5 at 235 °C.
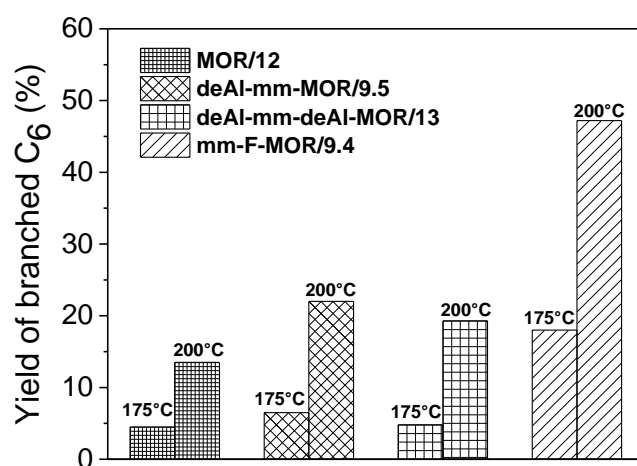
Figure 10. Comparison of the effects of the postsynthesis alkaline-acid (Pt/H-deAl-mm-MOR/9.5), acid-alkaline-acid (Pt/H-deAl-mm-deAl-MOR/13), and fluorination-alkaline (Pt/H-mm-F-MOR/9.4) treatments on the yields of branched hexanes at 175 and 200 °C.
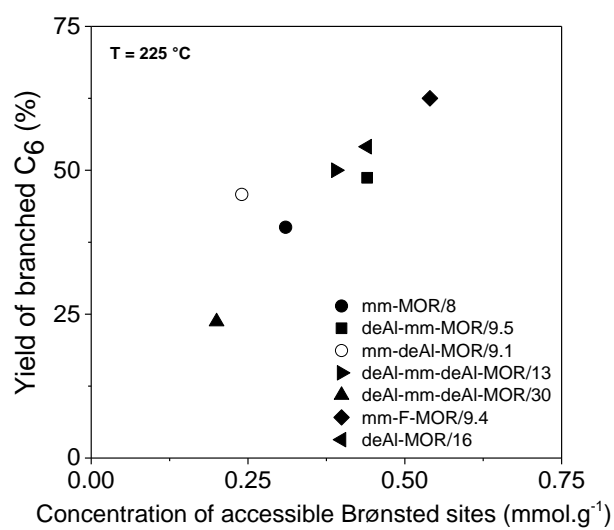
Figure 11. The yields of branched C$_6$ isomers in the hydroisomerization of *n*-hexane for Pt/H-MOR zeolites with different concentrations of the accessible Brønsted sites.

Graphical abstract